THE JOURNAL OF PHYSICAL CHEMISTRY C

pubs.acs.org/JPCC Article

Capturing the Iron Carburization Mechanisms from the Surface to Bulk

El Tayeb Bentria,* Salawu Omotayo Akande, Charlotte S. Becquart, Normand Mousseau, Othmane Bouhali, and Fedwa El-Mellouhi*

Cite This: J. Phys. Chem. C 2020, 124, 28569–28579 Read Online

ACCESS | Metrics & More | Article Recommendations | Supporting Information

ABSTRACT: Reactive force field molecular dynamics is a powerful tool to simulate large-scale reactive events such as catalytic reactions and metallic corrosion, including the carburization or so-called metal dusting corrosion. Building on a vast set of reactive force field parameters, it aims to reduce the gap between computational and experimental observations. However, the production of different versions of reactive force field parameter sets in the past 2 decades demonstrates the challenges faced by developers when attempting to describe correctly and at the same time a broad range of environments, such as the kinetics of CO adsorption, dissociation, and carbon diffusion in iron systems. This has limited the ability of these force fields to capture the competing phenomena governing complex evolution such as the carburization of iron responsible for metal dusting corrosion. In this work, we demonstrate that it is possible to treat very different environments in an integrated way by expanding the ReaxFF parameter set, creating an environment-specific description. This approach enables us to capture both metallic surface-induced dissociation of carbon-containing gases such as carbon monoxide (CO) and atomic carbon bulk diffusion in iron systems within the same simulation setup so far unreachable with previously available force fields. Employing this extended-ReaxFF to describe a cell containing a gas mixture of carbon monoxide and argon reacting with an Fe(110) surface, we fully capture at the same time competing carburization reaction/diffusion processes on both the surface and the bulk. Analysis of the radial distribution function and charge density maps shows a variety of carbon bonds at different stages/layers, highlighting the diversity of the mechanisms captured while using our extended-ReaxFF. Interestingly, at a CO coverage higher than 0.7 monolayers, the atomic arrangement of the iron atoms is sufficiently altered to cause surface reconstruction leading to a significant increase in carbon diffusion. Moreover, we are able to observe and quantify the diffusion of Fe from the bulk toward the upper coke layer, computationally elucidating the slow but continuous coke formation reported experimentally, opening a wide range of opportunities to model various stages of iron carburization mechanisms.

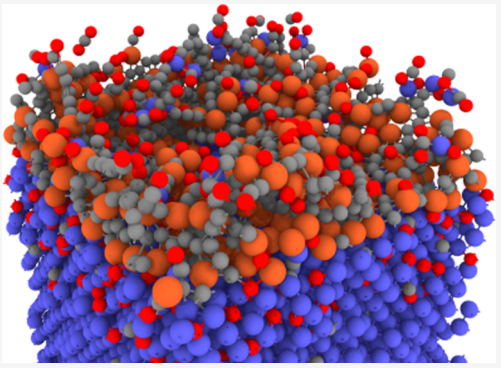

1. INTRODUCTION

Many complex reactions and surface phenomena are happening at the nanoscale level over time scales ranging from a few femtoseconds to nanoseconds that are difficult to capture using even the most advanced experimental characterization techniques.[1] For those phenomena, atomistic simulations are often the best characterization tools available. Yet, these have their own limitations: while *ab initio* quantum mechanical methods offer a high-quality description of the interactions and energies, they are too computationally expensive for problems such as corrosion, which require following the evolution of thousands of atoms over nanoseconds and more. Because of these requirements, molecular dynamical (MD) simulations must therefore be performed using semiempirical descriptions, in spite of their limited transferability. The embedded-atom method (EAM) created by Daw et al.,[2] for example, can reproduce the structural, physical, elastic, surface, and thermal properties for some simple materials[3] but cannot deal well with chemical reactions. Within the semiempirical method range, reactive force fields such as ReaxFF, with its bond-order formalism in conjunction with polarizable charge descriptions, offer a reasonably good description of both reactive and nonreactive interactions between atoms. Despite being computationally demanding if compared to EAM, ReaxFF remains relatively low cost compared to *ab initio* methods and offers a robust description of hydrocarbon chemistry,[4] as it has been used to address many phenomena occurring on scales that were previously inaccessible with heavier computational approaches.[5] ReaxFF enables us to perform simulations that

Received: October 6, 2020
Revised: December 7, 2020
Published: December 21, 2020

https://dx.doi.org/10.1021/acs.jpcc.0c09001
J. Phys. Chem. C 2020, 124, 28569–28579

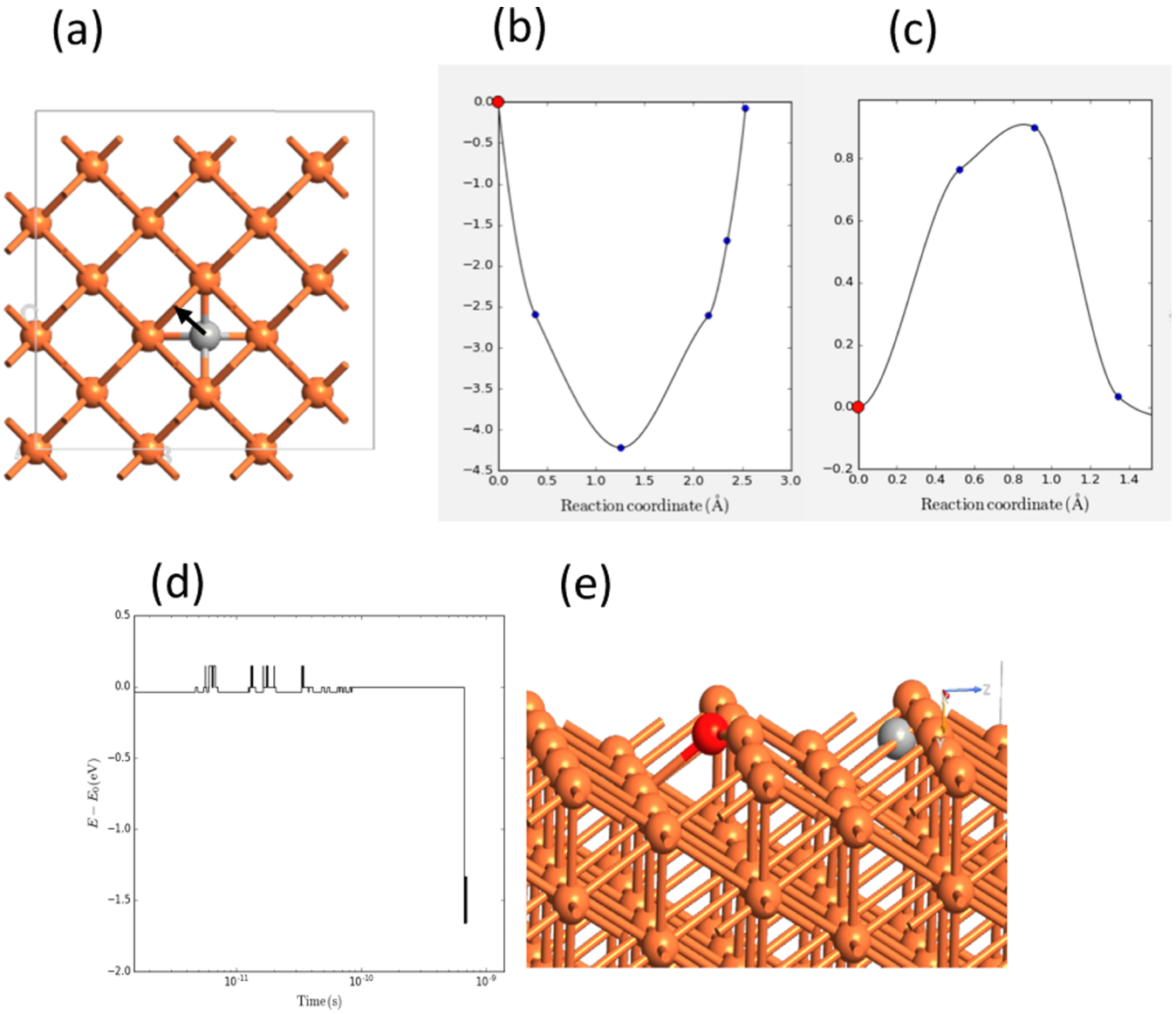

Figure 1. (a) Carbon diffusion pathway in bulk iron from one octahedral site to another octahedral site. Calculated migration pathways using NEB with (b) ReaxFF-2012 and (c) RPOIC-2017 semiempirical potentials. (d) Energetics of CO molecule dissociation on the Fe(110) surface calculated using RPOIC-2017 employed within the adaptive kinetic Monte Carlo (AKMC). (e) Snapshot of the stable configuration after an AKMC run showing the unphysically short Fe−C bond. Ball and stick atomic representation: iron (orange), oxygen (red), and carbon (gray). Results are generated using quantum ATK.[16,17]

involve reactive events at the interface between solid, liquid, and gas phases such as metal dusting corrosion.[6]

Metal dusting is a severe type of corrosion resulting from the uncontrolled catalytic reaction of hydrocarbons with metallic surfaces such as in reactors and pipelines at high temperatures. It results in a form of corrosion due to the decomposition of metal surfaces to dust particles (coke). Numerous experimental studies of dusting corrosion,[7−9] provided valuable qualitative and quantitative insights into the carburization process for metallic systems exposed to high carbon activity gas. Still, the early stage of iron carburization remains challenging to capture and control during experiments, calling for the need of atomistic simulations.

The hydrocarbon ReaxFF interatomic potential was first parameterized by van Duin et al.[5] and included the van der Waals and Coulomb forces. Over the years, various enhanced parameter sets, applicable to a wide range of applications and materials, were published.[6−9] For systems associated with the metal dusting phenomena of iron, ReaxFF predicts reasonable values for the dissociation of hydrocarbon molecules on iron surfaces.[10−12] Despite this success, these hydrocarbon/Fe potentials are unable to simulate carbon diffusion to the bulk due to rare or even no intrusion of carbon to the first or second iron subsurface layer, as reported in our earlier and other works.[3,13] Consequently, in 2017, Lu et al. proposed a new version of ReaxFF that simulates well carbon diffusion in bulk iron (this new version is denoted here as RPOIC-2017).[3]

One of the main advantages of reactive force fields is their transferability; for example, an oxygen atom is treated with the same mathematical formalism whether oxygen is in the gas phase as CO or incorporated into a solid phase. Such transferability allows ReaxFF to consider phenomena dependent not only on the reactivity of the involved species but also on dynamic factors, such as diffusivity and solubility, affecting

https://dx.doi.org/10.1021/acs.jpcc.0c09001
J. Phys. Chem. C 2020, 124, 28569−28579

how species migrate through the system. This makes it possible, in principle, to model complex processes involving multiple phases and interfaces. In practice, however, many interactions are much less transferable than expected. For example, while the description of hydrogen and oxygen atoms seems to account for a wide range of environments, it appears not to be the case for carbon within our system of interest due to its more complex chemistry.[14] Carbon potential transferability has been a persistent issue when trying to simulate at the same time carbon adsorption, dissociation, and diffusion in iron using different versions of ReaxFF. Sahputra et al.[14] have examined the potential developed by Islam et al. and demonstrated that the 2012 force field (denoted here as ReaxFF-2012)[12] is better suitable for reaction at iron surfaces but less suitable for subsurface and bulk diffusion properties. This is true, despite the fact that during their initial parameterization, Zou and van Duin[15] considered the equations of state (EOS) of carbides such as Fe_3C and the surface energy of Fe_5C_2.[15,15] Hence, it is likely that the inability of different versions of ReaxFF to predict at the same time carbon adsorption, dissociation, and diffusion is not due to the potential refitting but to the ReaxFF formalism itself. Indeed, the amount of information stored in the ReaxFF, more specifically in the off-diagonal parameters, might be insufficient to incorporate the wide variety of high and low coordination bonds that carbon can form, thus limiting the predictivity/transferability of such potentials.

In Section 2, we show how ReaxFF-2012 and RPOIC-2017 potentials struggle to predict both adsorption and diffusion at the same time and propose a solution called "extended-ReaxFF" to resolve this issue. We subsequently challenge the newly formulated potential in simulation setups mimicking experimental conditions to capture the iron carburization mechanism from the surface to bulk.

2. DESCRIPTION OF THE MODELS AND SIMULATION METHODOLOGY

2.1. Extended-ReaxFF. Here, we examine two of the well-known potentials designed to simulate the interaction of hydrocarbon molecules with iron systems, namely, ReaxFF-2012 and RPOIC-2017 potentials. We explain the major differences and limitations and propose a way to lift them. Figure 1a compares the carbon diffusion pathway from an octahedral site to another octahedral site (presented by the arrow in Figure 1a) in bulk Fe, computed using the nudged elastic band method (NEB) and the two force fields using quantum ATK.[16,17]

The negative barrier predicted by ReaxFF-2012 (Figure 1b) is unphysical, as discussed in ref 14, preventing it from correctly reproducing the carbon diffusion from the iron surface to the subsurface. RPOIC-2017, on the other hand, fails to describe the surface phenomena but predicts the correct bulk carbon diffusion barrier of 0.86 eV (Figure 1c) in good agreement with experimental and theoretical findings.[14,18] The fundamental parameter affecting the diffusion barrier is associated with the off-diagonal parameters of the van der Waals radius (R_{vdW}). Lowering the R_{vdW} parameter from 1.23 to 0.38 increases the carbon coordination and its ability to bond in a bulk-like environment like when a carbon atom occupies an octahedral site. Turning to the impact of lowering R_{vdW} on surface properties, we report the following: (i) for a CO molecule adsorbed in the bridge position, a negligible difference can be noticed in the measured Fe−CO bonds using both versions of the ReaxFF; and (ii) for a CO molecule adsorbed on a low coordination site such as the on-top position, the Fe−CO bond shrinks to an unrealistically low value of 0.7 Å.

To clarify further the Fe−C bonding issue in RPOIC-2017, we use an adaptive kinetic Monte Carlo (AKMC) technique[19] to investigate the CO dissociation events generated using this potential (Figure 1d). Upon CO dissociation, i.e., when the carbon atom moves to a low coordination position, the system encounters an unphysical reduction in energy of 1.5 eV caused by the formation of a very short Fe−C bond of 0.7 Å. This has a significant effect on the system as it lowers drastically the accuracy of adsorption and dissociation energetics for some cases, as shown in ref 3. Our attempt to refit the RPOIC-2017 potential by varying up to 51 parameters using SCM software[20] turned out to be inconclusive. The resulting refitting parameter sets led to R_{vdW} and vdW parameters fitted back to values close to those of ReaxFF-2012, which makes the newly fitted potential lose the advantageous bulk diffusion characteristic of RPOIC-2017 in favor of better surface dissociation energies. It appears that ReaxFF with its present formalism seems to be unable to simulate correctly and simultaneously both high and low carbon coordination since there is only one carbon type in ReaxFF to deal with different local chemical environments. Unlike popular nonreactive force fields like AMBER[21] and CHARMM,[22] ReaxFF does not employ atom tagging[6] due to the missing description of particles' self-interaction.[23]

Ideally, the adsorption and dissociation of hydrocarbon on the iron surface as well as carbon atom diffusion to the bulk could be achieved by building an entirely new reactive potential that would incorporate all kinetic phenomena of interest to simulate correctly the carburization of iron. Machine learning (ML) potentials could be good candidates: Deringer et al. demonstrated that a potential built using this strategy could incorporate different atomic hybridizations of carbon atomic orbitals from sp1 up to sp3.[24] Unfortunately, this approach has worked only so far to build elemental atomic potentials such as pure iron[25] and pure carbon.[24] The complexity of the catalytic reaction of interest in this work requires a large amount of data, where the elements are in very different environments and bonding situations. At the moment, it seems difficult to build and trust ML potentials to reproduce and predict good results for a system such as Fe−C in the near future.[26]

Taking advantage of the robust formalism of ReaxFF and its stable and scalable implementation in various molecular dynamics simulation tools such as the large-scale atomic/molecular massively parallel simulator (LAMMPS) seems to be the best option for now. Hence, we propose a new approach to extend the ReaxFF parameter sets by tagging the host Fe atoms. This enables us to distinguish between low (surface iron Fe_S) and high (bulk iron Fe_B) coordination regions recognizable for adsorbates and impurities such as carbon. Our simulation box containing an iron slab is divided along the z-direction into two spatial regions, as shown in Figure 2. Region 1 includes the vacuum space down to the first layer of Fe; therein, iron atoms are tagged as Fe_S and will be treated with the Fe/C/O ReaxFF-2012 potential parameter set. Region 2 corresponds to iron bulk excluding the first Fe layer. All Fe atoms in region 2 are tagged as Fe_B, while the interactions are described using the Fe/C/O RPOIC-2017 parameterization. Our extended-ReaxFF formalism implies that the interactions between atoms in the upper region are treated by ReaxFF-

https://dx.doi.org/10.1021/acs.jpcc.0c09001
J. Phys. Chem. C 2020, 124, 28569−28579

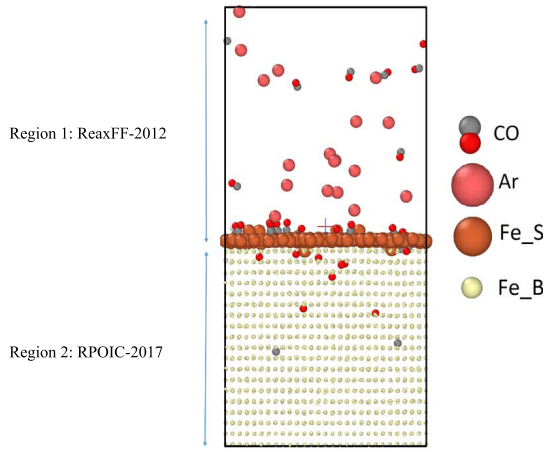

Figure 2. Computational model used in this work containing around 5100 Fe atoms. The Fe atoms in the first layer are called Fe_S and the rest, Fe_B. In our extended-ReaxFF formalism, the interactions between atoms in the upper region are treated by ReaxFF-2012, while the Fe atoms in the bottom region are treated by RPOIC-2017. The vacuum is filled with a flowing gas mixture of CO molecules (gray and red balls) and Ar (large red balls).

2012, while those in the bottom region are treated by RPOIC-2017. This approach allows us to correctly capture a smooth transition from low to high coordination during carbon diffusion from the surface to the bulk. It is worth noting that interactions between the tagged Fe_B, Fe_S and other reactive species are also added to the parameter set. The interaction between Fe_B and Fe_S is handled by adding to the ReaxFF parameter file the needed diagonal, off-diagonal, angle, and torsion parameter sets.

Fe_S−Fe_S, Fe_B−Fe_B, Fe_B−Fe_S, and Fe_S−Fe_B bond interaction parameter sets are not impacted by tagging iron interactions and are all similar, taking the common values for Fe−Fe bonds in both ReaxFF-2012 and RPOIC-2017 potentials. For parameterizing angles and torsion terms, we used the same common parameterization as in ReaxFF-2012 and RPOIC-2017 potentials. The off-diagonal terms that define both bond order and van der Waals pair interactions have been set to −1.0000. This means that we call ReaxFF to compute these terms using an embedded combination rule between the atomic parameter.[23] When tested, the parameterization described above gives excellent results for handling mixed Fe_S and Fe_B surface and bulk systems (see Figures 2 and S5).

To alleviate the computational burden and discontinuities caused by sudden changes in velocities and forces, we do not alter the tagging of Fe atoms in the course of the simulation; instead, we tag Fe atoms as Fe_S or Fe_B only at the beginning of the simulation and let the system evolve. There should be no alteration of the dynamic if a single Fe_S moves to the bulk or a single Fe_B moves to the surface. The only case where we foresee the appearance of some artifacts could be if a cluster of Fe_B forms on the surface to create a bulk-like environment that interacts with CO_2. This scenario is very

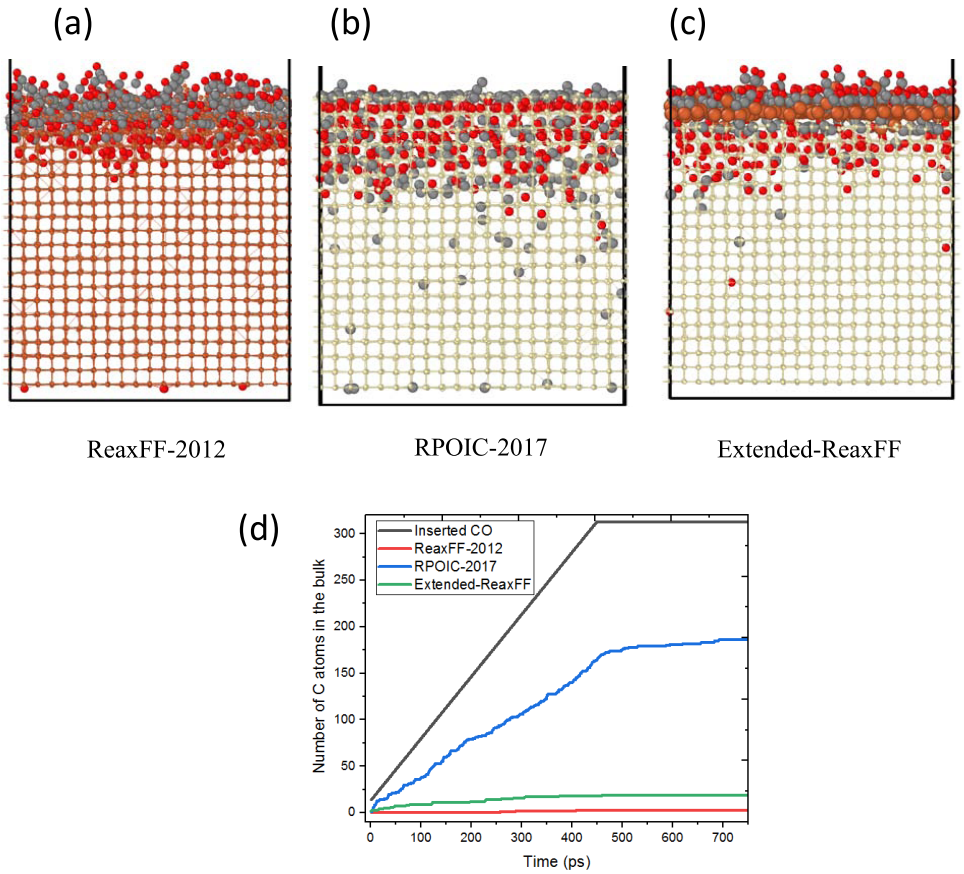

Figure 3. Screenshot of the final frame of simulation after 750 ps and T = 773 K, using three different potentials: (a) ReaxFF-2012, (b) RPOIC-2017, and (c) our extended potential extended-ReaxFF. (d) Evolution of the number of C atoms loaded in iron bulk as a function of the simulation time using the three force fields.

https://dx.doi.org/10.1021/acs.jpcc.0c09001
J. Phys. Chem. C 2020, 124, 28569−28579

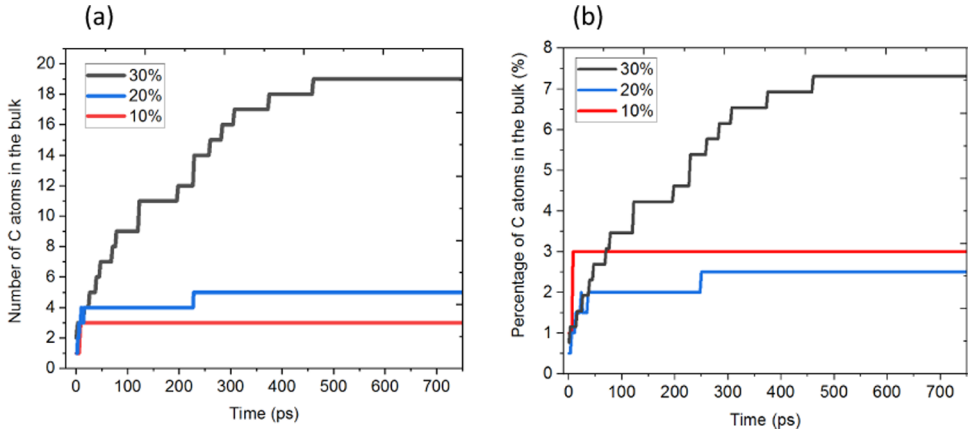

Figure 4. Carbon diffusion into iron bulk at T = 773 K as a function of the simulated time for different gas mixtures with CO concentrations of 10, 20, and 30%. (a) Total number of C atoms that have diffused and (b) percentage of C atoms that migrated into the bulk.

unlikely to occur since Fe is very reactive with the other species, and if, in rare instances, it travels to the surface, it does as an individual atom and is very unlikely to segregate.

2.2. Computational Details. Molecular dynamics (MD) simulations are performed using the LAMMPS code.[27] We build a periodic simulation box containing a (110) iron slab of 43 × 49 × 40 Å^3 accounting for around 5100 Fe atoms with 90 Å vacuum along the z-direction. Iron atoms are tagged as Fe_S and Fe_B depending on the surface/bulk definition, respectively. The "deposit" command of the LAMMPS package is used to insert the gas molecules into the vacuum region lying above the slab. This feature allows the simulation of gas flow and the insertion of molecules randomly positioned in the vacuum every n time steps. To mimic experimental settings, gas mixtures contain different concentrations of CO molecules (10−30%), while the remaining (90−70%) consists of argon inert molecules[28] that enable maintaining similar gas pressure for all studied systems. More precisely, a molecule is inserted every 1.5 ps (6000 MD steps) with an initial molecular speed of 0.0001 Å/fs parallel to the slab surface, giving rise to a flux of 100 m/s, which is the maximum gas flow speed in controlled pipelines.[29] To avoid inserting particles close to the surface and a brutal evolution at the beginning of the simulation, the CO insertion is kept 10 Å away from the surface and its periodic counterpart while the insertion rate is controlled based on the desired reactive gas concentration. After CO molecular dissociation, a carbon atom is considered as having diffused only if it moves 2 Å below the initial surface.

To converge more toward a real-case scenario, after relaxation in a constant number of particles, pressure, and temperature (NPT ensemble) for 10 000 steps at 10 K, the system is heated up gradually to the desired temperature in the NVE (constant number of particles, volume, and energy) ensemble by steps of 0.01 K to reach the target temperature of 773 K. This target temperature corresponds to the critical carbon steel carburization temperature before entering into the metal dusting regime according to the experimental observation of Grabke et al.[9] Once the desired temperature is reached, the system is once more relaxed for 5000 steps under NPT conditions and molecule insertion is initiated afterward. We find that this procedure leads to high stability with NPT ensemble for large-scale systems and is more convenient compared to NVT settings that cannot allow us to simulate correctly the phase transitions from pure iron to iron carbides/oxides.

3. RESULTS

To test the reliability of the newly extended potential, we investigate the simultaneous adsorption, dissociation, and diffusion of carbon monoxide molecules on an iron surface, a simple but fundamental process for the initiation of metal dusting corrosion.[30] Figure 3 shows the snapshots of the final frames after 3 million steps of MD for a total time of 750 ps. Force and velocities are computed using the three potentials (a) ReaxFF-2012,[15] (b) RPOIC-2017,[3] and (c) our extended-ReaxFF. MD simulations using ReaxFF-2012 (Figure 3a) evolve in a similar way to our previous work.[31] It is clear from the final frame that, in the course of the simulation, several events of CO dissociation occurred, followed by carbide complex formation causing the supersaturation of the surface. No carbon diffusion into the iron bulk can be noticed, whereas oxygen diffusion reaches up to the fourth layer. In the MD simulations using RPOIC-2017 (Figure 3b), CO dissociates readily on the iron surface and diffuses into the iron slab. The end of this simulation consists of an iron sample loaded with carbon and oxygen that diffused deep into the sample. In the course of this later simulation, it is not possible to observe the well-known mechanisms of CO adsorption, tilt, and dissociation.[32] The speedy CO dissociation we obtained looks unrealistic in such a short simulation time (taking into consideration that the CO dissociation barrier of the Fe (110) surface is ∼0.8 eV)[31] and led to the complete diffusion of all C and O atoms into the bulk. It is noticeable that C prefers to relax in high coordination positions, causing the first layers of the iron slab to become highly loaded with O and C (Figure 3b).

By simulating the simultaneous adsorption, dissociation, and diffusion of carbon monoxide molecules on iron surfaces using extended-ReaxFF (Figure 3c), one can notice, from the final frame, that 6% of carbon atoms in the system diffused into the subsurface or even the bulk with the persistence of some undissociated CO molecules on the iron surface, which is the expected behavior as discussed earlier. Figure 3d presents the number of carbon atoms that diffused from the surface to the bulk out of the total number of inserted CO molecules in the gas mixture as a function of time for the three systems. Let us recall that we consider that a carbon atom has diffused into the bulk as soon as it reaches the third layer of the iron slab. A comparison between the curves in Figure 3d clearly demonstrates the differences between the different potentials

https://dx.doi.org/10.1021/acs.jpcc.0c09001
J. Phys. Chem. C 2020, 124, 28569−28579

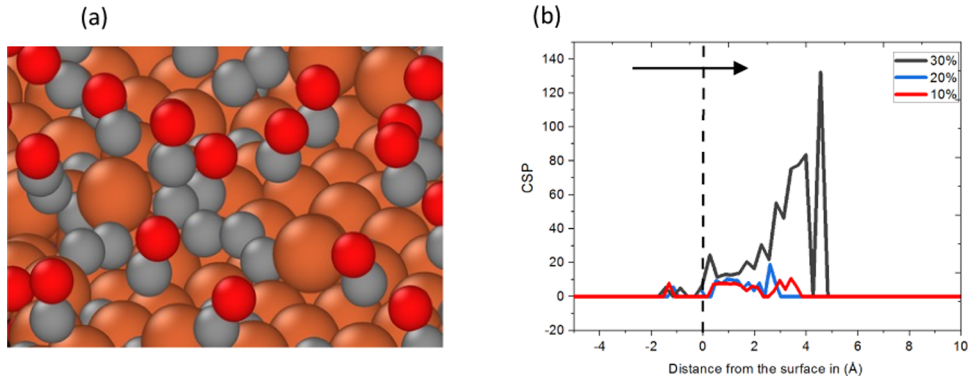

Figure 5. (a) Snapshot of the Fe surface exposed to 30% CO after 300 ps. (b) Centrosymmetry parameter (CSP) for the Fe_S atoms with respect to their neighbors along the *z*-axis. Analysis was processed on the last frame of MD simulations (800 ps) of Fe(110) surfaces exposed to gas mixtures containing 10, 20, and 30% CO gas filled with argon. In this figure, the origin ($z = 0$) is set at the Fe(110) surface, namely, at the atoms tagged Fe_S. The black arrow indicates the direction from the Fe bulk to the gas region.

we highlighted earlier and shows that the extended-ReaxFF is capable of capturing smoothly the simultaneous dynamics of surface and bulk reactions. Further checkpoints were validated by calculating the relevant CO dissociation and C diffusion pathways using the extended-ReaxFF and the NEBs presented in Figures S1 and S2. The computed barriers are in agreement with the well-known CO dissociation and C diffusion computed from density functional theory (DFT) calculations and give us confidence on the continuity of energies.[3,31] The Fe−C bonding in the bulk, however, needs further improvement as the carbon atom occupies pseudo-octahedral sites. More enhancement on the extended-ReaxFF will be conducted in the future as the ReaxFF parameterization is out of the scope of this work.

To investigate the impact of CO concentration on C diffusion into the bulk, we apply the new extended potential to simulate the experimental conditions of iron carburization conducted by Grabke et al. in 1994.[9] The setup of our MD simulation is the one described in Section 2.2. Figure 4a reports the number of carbon atoms that diffused into the bulk as a function of the simulation time, where Figure 4b represents the percentage of C atoms that migrated into the bulk from the total carbon concentration in the gas. For a gas mixture with an initial CO concentration lower than 20%, corresponding to a coverage below 0.58 monolayers (MLs), up to 3% of the C resulting from the CO dissociation did diffuse into the bulk iron. When the CO concentration increases to 30%, corresponding to a coverage of 0.78 ML, the ratio of diffusing C is higher, reaching almost 8%. This trend is in qualitative agreement with the experimental findings of Grabke et al. reporting a mass gain (due to carbon deposit and cementite formation) of 7, 13, and 37 mg/cm^2 for CO concentrations of 10, 20, and 30%, respectively.[9] It should be noted that performing the same simulations with or without argon leads approximately to the same results, meaning that it is the CO partial pressure and not the total pressure that has the biggest influence on this phenomenon.

4. DISCUSSION

In this section, we discuss the results obtained, elucidate the mechanisms affecting the increase of CO partial pressure in metal dusting corrosion, and discuss some phenomena occurring during dusting corrosion.

4.1. Surface Reconstruction: A Key Mechanism in Metal Dusting Corrosion. To understand why the increase in CO content leads to a higher diffusion rate, we analyze the surface morphology at the final state of our simulations. Even after 300 ps of the simulation time, where 10% of CO molecules have been inserted and relaxed on the surface, the iron surface atoms (Fe_S) still occupy positions close to their perfect arrangement. The same is observed for the simulation with 20% CO molecules. This CO concentration did not alter the well-arranged Fe structure at the surface. However, for 30% CO, the surface properties changed considerably. The effect of CO concentration on dissociation barriers has been discussed based on DFT results in ref 32. They reported a dissociation barrier change from 0.78 eV for a coverage of 0.0625 ML to 1.64 eV for a coverage of 0.25 ML in disagreement with experimental observations[9] and this MD study. The high dissociation barrier at a high concentration obtained using DFT is expected due to the small unit cells used to simulate the high C concentrations (2 × 2 Fe unit cells), which constrain the CO molecular movement with its periodic image. This is not the case in our larger MD systems where CO molecules can act independently and so can the Fe atoms. Figure 5a shows a snapshot of the surface after 300 ps, where the beginning of the formation of C−C chains and the reconstruction of the iron surface induced by the surrounding C atoms can be noticed. We showed, however, in our latest study that step edges that can be generated after surface reconstruction provide even lower dissociation barriers of 0.54 eV,[31] the iron reconstruction on the surface provides a step edge-like environment that may contribute to the higher dissociation/diffusion rate in the 30% case.

To study the correlation between surface reconstruction and carbon diffusion, we calculated the centrosymmetry parameter (CSP) of the Fe surface using the Ovito visualization tool.[33] The CSP is defined as follows

$$\mathrm{CS} = \sum_{i=1}^{N/2} |R_i + R_{i+N/2}|^2$$

where N is the nearest neighbors of each atom. R_i and $R_{i+N/2}$ are the vectors from the central atom to a particular pair of the nearest neighbors. In a perfect crystalline system, these vectors cancel each other, leading to CSP = 0. This parameter is thus a useful measure of the local lattice disorder around an atom, suitable to quantify the reconstruction of atoms when the

https://dx.doi.org/10.1021/acs.jpcc.0c09001
J. Phys. Chem. C 2020, 124, 28569−28579

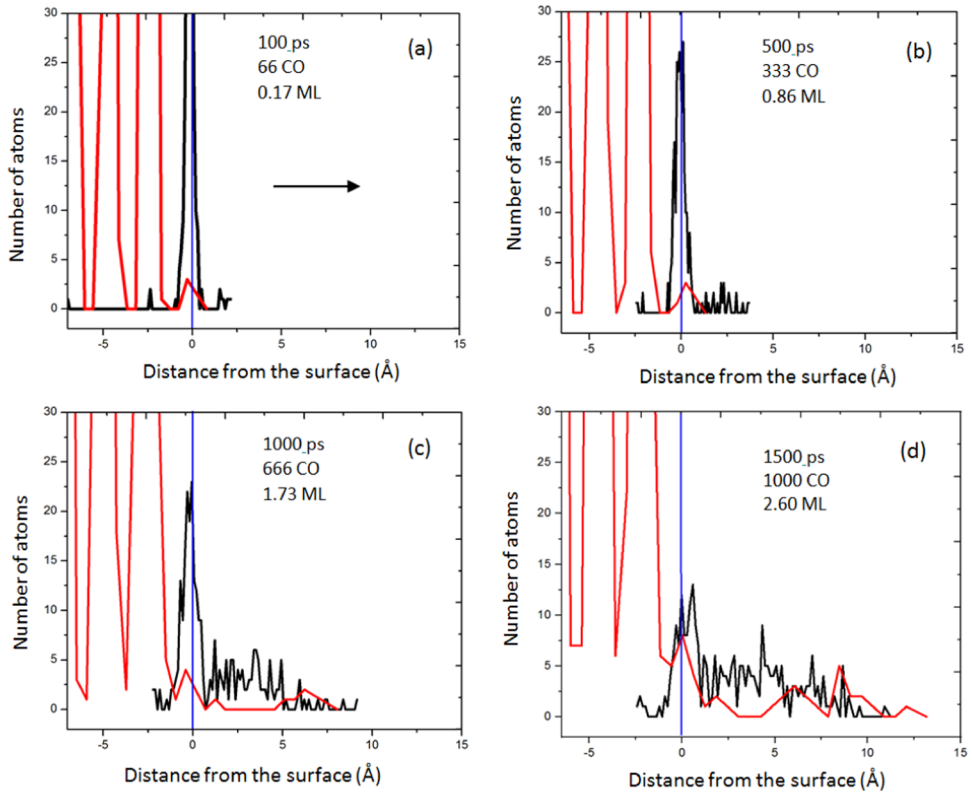

Figure 6. Linear distribution function for iron bulk atoms (Fe_S in black) and iron surface atoms (Fe_B in red), at different simulation times, with the insertion of CO molecules every 6000 steps leading to a total of 1000 CO molecules inserted at T = 773 K. The black arrow indicates the direction from the bulk to the gas region.

structure deviates from the perfect body-centered cubic (BCC) structure.[34] It can be used also to characterize whether the atom is part of a perfect lattice, a local defect, or at a surface. Figure 5b presents the CSP values for Fe_S atoms as a function of the neighbors along the z-coordination. In this figure, the origin (z = 0) is set at the Fe(110) surface, namely, at the atoms tagged Fe_S. The results show clearly that the 0.7 ML CO surface coverage (originating from a 30% CO gas concentration) is able to disrupt the arrangement of the perfect iron surface and cause reconstruction that moved Fe atoms up to 5 Å above the surface, thus creating vacancy defects on the surface. This also implies that it is exposing more catalytic sites for CO adsorption and C diffusion.[35] These results confirm that the CO concentration (partial pressure) is a key factor for corrosion since CO-containing gases can disrupt well-manufactured metal surfaces at the temperatures of interest.

4.2. Iron Diffusion from Bulk to Surface. The continuation and evolution of metal dusting corrosion reaction are related experimentally to the fresh catalyst particles (Fe) diffusing from the bulk to the surface.[36] Pippel et al.[37] showed that at advanced stages of the metal dusting process, the decomposition of the metastable cementite layer is a continuous process that leads to the formation of carbon filaments (coke) with a metallic tip that is responsible for further carbon deposition and the growth of filamentous carbon nanotubes. The thickness of the coke layer increases to tens of micrometers driven by the catalytic activity of the metal particles diffusing slowly from the deeper layers to the surface. Simultaneously, the cementite grows toward the interior of the metal sample due to the diffusion of carbon from super-saturated regions toward the metal, resulting in a steady-state cementite thickness of 1−2 μm.[38] This phenomenon, while observed experimentally,[39] has, to the best of our knowledge, seldom been captured or reported computationally. As demonstrated in Section 4.1, the setup of our simulations using the extended-ReaxFF allows us to investigate this crucial carbon and iron interdiffusion through the metallic surface during the carburization process.

We attribute this success to the ability to differentiate between surface and iron atoms achieved through the different tagging of the iron atoms depending on their position (bulk/surface). This gives us the possibility to differentiate the diffusion of atoms tagged as Fe_B atoms from those tagged as Fe_S. Encouraged by this success, we continued to increase the concentration of CO in the sample to boost and observe the advanced stages of iron carburization by inserting additional CO molecules every 1.5 ps, until we reached a total of 1000 CO molecules at a total simulation time of 1500 ps. Figure 6 presents the linear distribution function of iron bulk and surface atoms along the z-direction and at different frames of the simulation generated using OVITO.[33] The blue lines indicate the initial reference position of the surface to help the reader follow the evolution of the surface during the carburization process and quantify the thickness of the coke layer formed. At 100 ps, some Fe_S atoms on top of the surface experience a mild reconstruction (please refer to the black curve in Figure 6a).

As time evolves, the surface iron atom reconstruction grows steadily due to the consumption of Fe_S atoms during the formation of metastable carbides and due to the increasing number of inserted CO molecules and the increasing coverage of the surface (refer to the black curve in Figure 6b−d). One

https://dx.doi.org/10.1021/acs.jpcc.0c09001
J. Phys. Chem. C 2020, 124, 28569−28579

can notice that toward the end of the simulation (at 1500 ps, Figure 6d) the diffusion of Fe atoms from the reference point toward the vacuum filled with CO molecules becomes sizable. A very similar drift of bulk iron atoms (Fe_B red curve) can be noticed as well by looking at the evolution of the system in Figure 6a−d. One might notice that Fe_B atoms move toward the vacuum filled with CO molecules and probably start working as a catalytic site to allow further CO decomposition. Toward the end of the simulation, a carbide layer reaching a thickness of ∼12.5 Å is formed, the composition of which is further analyzed in Section 4.3. It is worth mentioning that the proper way to run the simulation is to run a script that checks the position of Fe_B every picosecond and change its type to Fe_S if the atom passes the surface layer and vice versa. This approach is not used in this paper to be able to observe the diffusion of Fe_B from the bulk to the surface. This allows for more realistic carbon adsorption and dissociation compared to the perfect surface. Overall, since individual Fe_S and Fe_B atoms move toward the vacuum region to participate in the formation of the carbides, we do not expect that their tagging influences the overall dynamics.

4.3. Carbide Phase Formation. To understand the composition of the carbide phases formed toward the end of the carburization simulation, we calculated the radial distribution function (RDF) to analyze the nature of bonding in our final Fe system. We also calculated the number of atoms per layer to show the composition of the phases produced in these systems. Figure 7 shows the change in the RDF for the

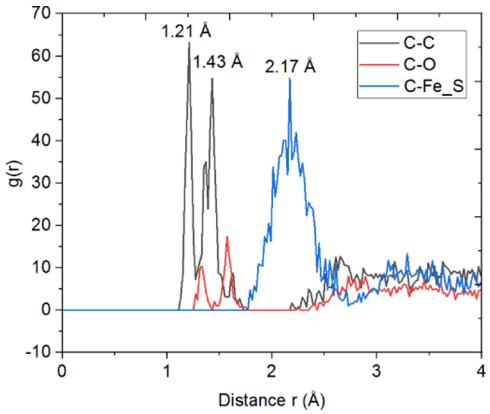

Figure 7. Radial distribution function (RDF), $g(r)$, for surface C bonds with Fe_S in blue, oxygen in red, and carbon in black at t = 1500 ps. $g(r)$ represents the probability of finding a particle at a distance r (Å).

atomic species composed of the carbide layer, namely, carbon, oxygen, and iron (both bulk and surface) atoms, excluding the gas molecules. Due to the simplicity of the model Fe/C/O, it is straightforward to conclude on the nature of bonding. The formation of double and triple carbon−carbon bonds is represented by the strong peaks at r = 1.21 Å corresponding to sp^3 bonding. The peaks at 1.35 and 1.43 Å correspond to graphene formation since double sp^2 C−C hybridization has a length of 1.3−1.45 Å,[40] which belongs to the coke phase (Figure 7). A wider peak with maximum intensity at 2.17 Å is observed and corresponds to a C−Fe single bond; the width of this type of bond coincides well with the cementite phase that forms bonds from 1.98 to 2.62 Å,[41] indicating the beginning of cementite formation in our system. Note that even though this simulation reached 6 million steps, which corresponds to 1500 ps, it is still relatively too short to observe a clear stabilization of cementite. The undissociated CO molecules attached to the coke layer are evidenced by the small red peaks at 1.32 and 1.60 Å, which can be related to a single C−O bond after the adsorption of carbon on the surface and CO molecules on their way to dissociate by forming weaker CO bond in the Fe−O−C−Fe complex, respectively.

The carbon and oxygen linear distribution functions in the Fe system per 1 Å thick slices, along the z-direction, for the simulation where 30% CO concentration was introduced at T = 773 K, are presented in Figure S7. The existence of two phases is visible. The first phase from the reference down to −10 Å beneath the surface is an oxygen-rich layer with a small carbon amount having diffused mainly at the beginning of the simulation when the surface was fresh (319 oxygen and 105 carbon at 500 ps, for example). The second layer above the reference of the surface is a carbon-rich layer, where carbon is at its highest concentration. At the top of the carbide layer, there are more carbon atoms than oxygen due to the fact that after CO molecule adsorption, oxygen atoms tend to stay at the top of the surface for a short time and get back to the vacuum by forming molecular oxygen or CO_2 while the carbon atoms tend to continue growing on the coke layer.

The biggest advantage of ReaxFF over the other potentials is its ability to calculate the charge density of each atom on the fly, which allows bonds to form and break.[4] This feature gives us the advantage of visualizing the large-scale MD metal dusting corrosion product and the charge density of each atom. Charge maps give an interesting visualization of the corrosion phenomenon as it underlines the bonding nature of specified regions. Figure 8a shows a snapshot of the system along the xz plane after 1500 ps and the introduction of 1000 CO molecules, and Figure 8b shows the charge density on the same system. The oxide layer that donates electrons is represented in blue, together with the diffusing C atoms in interstitial sites that also donate electrons. The carbide (C + Fe) has a positive charge (taking electrons from the iron atoms); thus, it is represented in red. Carbon filaments are observed (see Figure 8a) in the coke layer. They have a neutral charge as expected due to their covalent C−C bond and are represented in green (Figure 8b). Correlating this charge visualization with experiments would help indicate how corrosion is attacking iron (red) and how the oxide layer might protect it (blue) from further carburization.[9] It is also possible to visualize the charge for different compounds separately. Figure S6 shows the case of carbon charges only along the xz plane. This figure shows that the carbon has a wide charge states ranging between −0.5 and 0.2 eV, based on the type of the bond formed, and illustrates the complicated and central role of carbon in metal dusting corrosion, as it exists with a positive charge in the gas phase and a negative charge with the carbide phases.

We have shown, with these few examples, how the extended reactive force field with its enhanced carbon adsorption and diffusion barriers opens the door to more accurate atomistic simulations of metal dusting corrosion. This is a problem that takes into account carbon diffusion leading to the correct atomic concentration at the surface/bulk and thus more accurate catalytic reactions at the surface. It should be noted that the use of only CO molecules only does not represent full metal dusting corrosion phenomena as hydrogen gas, water, and even sulfides are often present in the gas mixture.

https://dx.doi.org/10.1021/acs.jpcc.0c09001
J. Phys. Chem. C 2020, 124, 28569−28579

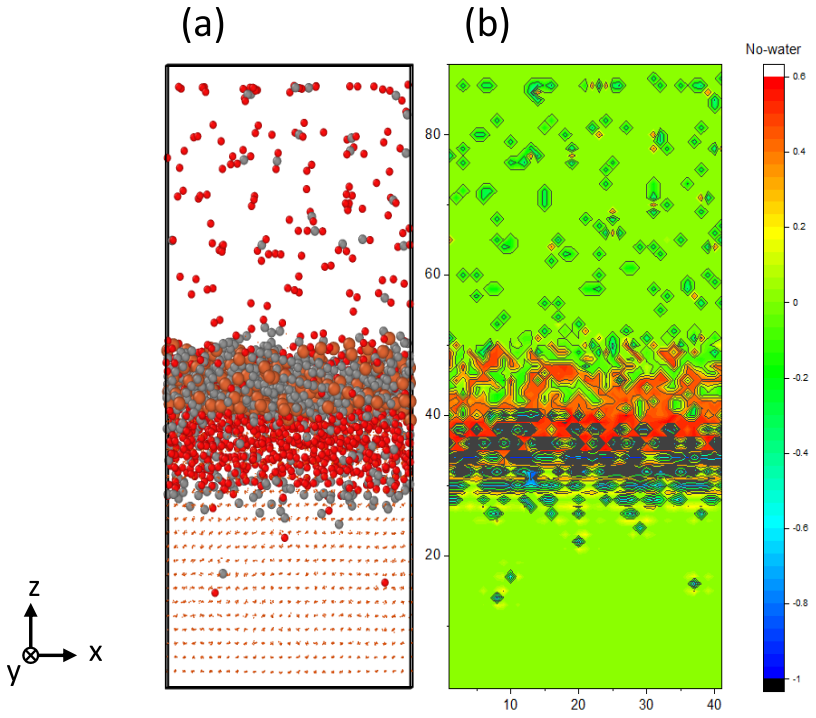

Figure 8. (a) Snapshot of the simulation at 1500 ps with an insertion of 1000 CO molecules. (b) Charge density map of the same system along the *xz* plane.

Potentially, the accuracy of the potential could be enhanced in the future by splitting the parameterization training set into a surface training set and a bulk training set and run the reparameterization in two steps. It is worth mentioning that the extended potential approach is valid only when it is possible to define clearly different environments, such as bulk and surface as in this example, where there is a need to describe the drastic changes in the coordination of carbon atoms; this approach is not valid if Fe_B are in low coordination position such as iron systems simulated at temperatures above the melting point, as we will fall back to the same issue RPOIC-2017 has.

5. CONCLUSIONS

In this paper, we succeeded in capturing the key iron carburization mechanisms involved in metal dusting corrosion of carbon steel, a serious corrosion issue encountered in the oil and gas industry. We showed that ReaxFF with its conventional formalism struggles to predict correctly the iron carburization responsible for initiating metal dusting corrosion observed in carbon steel. The carburization evolves under diverse environments, namely, surface adsorption of carbides followed by C diffusion toward the bulk, requiring that C moves from a lower-coordinated surface environment to a higher-coordinated bulk state. We lift this limitation by extending the standard parameter setup to allow specific adaptation to the interactions of carbon at the surface and in the bulk separately. We tested the extended potential using molecular dynamics simulations of an iron surface exposed to a flowing gas mixture containing various CO concentrations at the experimentally reported temperature of 773 K that record the acceleration of metal dusting corrosion.

We demonstrate that our simulations are able to reproduce reasonably well, and at the same time, the CO adsorption and dissociation at the surface, as well as the diffusion into the bulk, accounting for the overall carbon insertion and diffusion processes. Interestingly, our simulations could also capture the experimentally observed diffusion of iron from the bulk to the surface when the concentration of CO molecules on the surface is high enough (above 0.7 ML). Structural analysis employing the radial and linear distribution functions indicates the formation of oxide and carbide layers. This is further confirmed by charge density map analysis that indicates the complexity of the reactions taking place during iron carburization, with carbon adopting a broad spectrum of charge states and coordination.

Beyond the study of C absorption in Fe, the insertion of multienvironment parameter set into ReaxFF opens the door to model new reactions and phenomena observed experimentally, often unreachable with other potentials such as diffusion of iron atoms from the bulk to the surface.

■ ASSOCIATED CONTENT

Supporting Information

The Supporting Information is available free of charge at https://pubs.acs.org/doi/10.1021/acs.jpcc.0c09001.

Nudged elastic band, bond length, charge map, and linear distribution function of carbon and oxygen in the iron system (Figures S1−S7) (PDF)

■ AUTHOR INFORMATION

Corresponding Authors

El Tayeb Bentria − *Qatar Environment and Energy Research Institute, Hamad Bin Khalifa University, Doha, Qatar*; Email: ebentria@hbku.edu.qa

Fedwa El-Mellouhi − *Qatar Environment and Energy Research Institute, Hamad Bin Khalifa University, Doha, Qatar*; orcid.org/0000-0003-4338-9290; Email: felmellouhi@hbku.edu.qa

https://dx.doi.org/10.1021/acs.jpcc.0c09001
J. Phys. Chem. C 2020, 124, 28569−28579

Authors

Salawu Omotayo Akande − *Texas A&M University at Qatar, Doha, Qatar*

Charlotte S. Becquart − *Univ. Lille, CNRS, INRAE, Centrale Lille, UMR 8207 UMET Unité Matériaux et Transformations, F-59000 Lille, France*

Normand Mousseau − *Département de Physique and Regroupement Québécois sur les Matériaux de Pointe, Université de Montréal, Montréal, Quebec, Canada H3C 3J7*

Othmane Bouhali − *Texas A&M University at Qatar, Doha, Qatar*

Complete contact information is available at: https://pubs.acs.org/10.1021/acs.jpcc.0c09001

Notes

The authors declare no competing financial interest.

■ ACKNOWLEDGMENTS

This work is supported by the Qatar National Research Fund (QNRF) through the National Priorities Research Program (NPRP) under Project Number NPRP10-0105-170118. The advanced computing facility of Texas A&M University at Qatar is used for all calculations. F.E.-M. and O.B. are thankful for fruitful discussions from Nick Laycock, Abitha Ramesh, Aarthi Thyagarajan, Wouter Hamer, Dhruv Arora, and Prathamesh Shenai from Shell.

■ REFERENCES

(1) Brodland, G. W. How Computational Models Can Help Unlock Biological Systems. *Semin. Cell Dev. Biol.* **2015**, *47*−*48*, 62−73.

(2) Daw, M. S.; Baskes, M. I. Embedded-Atom Method: Derivation and Application to Impurities, Surfaces, and Other Defects in Metals. *Phys. Rev. B* **1984**, *29*, No. 6443.

(3) Lu, K.; He, Y.; Huo, C.-F.; Guo, W.-P.; Peng, Q.; Yang, Y.; Li, Y.-W.; Wen, X.-D. Developing ReaxFF to Visit CO Adsorption and Dissociation on Iron Surfaces. *J. Phys. Chem. C* **2018**, *122*, 27582−27589.

(4) Islam, M. M.; Zou, C.; van Duin, A. C. T.; Raman, S. Interactions of Hydrogen with the Iron and Iron Carbide Interfaces: A ReaxFF Molecular Dynamics Study. *Phys. Chem. Chem. Phys.* **2016**, *18*, 761−771.

(5) van Duin, A. C. T.; Dasgupta, S.; Lorant, F.; Goddard, W. A. ReaxFF: A Reactive Force Field for Hydrocarbons. *J. Phys. Chem. A* **2001**, *105*, 9396−9409.

(6) Senftle, T. P.; Hong, S.; Islam, M. M.; Kylasa, S. B.; Zheng, Y.; Shin, Y. K.; Junkermeier, C.; Engel-Herbert, R.; Janik, M. J.; Aktulga, H. M. The ReaxFF Reactive Force-Field: Development, Applications and Future Directions. *npj Comput. Mater.* **2016**, *2*, No. 15011.

(7) Szakálos, P. *Mechanisms of Metal Dusting*; KTH, 2004.

(8) Young, D. J.; Zhang, J.; Geers, C.; Schütze, M. Recent Advances in Understanding Metal Dusting: A Review. *Mater. Corros.* **2011**, *62*, 7−28.

(9) Grabke, H. J.; Bracho-Troconis, C. B.; Müller-Lorenz, E. M. Metal Dusting of Low Alloy Steels. *Mater. Corros.* **1994**, *45*, 215−221.

(10) Chenoweth, K.; van Duin, A. C. T.; Goddard, W. A. ReaxFF Reactive Force Field for Molecular Dynamics Simulations of Hydrocarbon Oxidation. *J. Phys. Chem. A* **2008**, *112*, 1040−1053.

(11) Mueller, J. E.; van Duin, A. C. T.; Goddard, W. A., III Development and Validation of ReaxFF Reactive Force Field for Hydrocarbon Chemistry Catalyzed by Nickel. *J. Phys. Chem. C* **2010**, *114*, 4939−4949.

(12) Zou, C.; van Duin, A. C. T.; Sorescu, D. C. Theoretical Investigation of Hydrogen Adsorption and Dissociation on Iron and Iron Carbide Surfaces Using the ReaxFF Reactive Force Field Method. *Top. Catal.* **2012**, *55*, 391−401.

(13) Bentria, E. T.; N'tsouaglo, G. K.; Becquart, C. S.; Bouhali, O.; Mousseau, N.; El-Mellouhi, F. The Role of Emerging Grain Boundary at Iron Surface, Temperature and Hydrogen on Metal Dusting Initiation. *Acta Mater.* **2017**, *135*, 340−347.

(14) Sahputra, I. H.; Chakrabarty, A.; Restrepo, O.; Bouhali, O.; Mousseau, N.; Becquart, C. S.; El-Mellouhi, F. Carbon Adsorption on and Diffusion through the Fe (110) Surface and in Bulk: Developing a New Strategy for the Use of Empirical Potentials in Complex Material Set-ups. *Phys. Status Solidi* **2016**, *254*, No. 1600408.

(15) Zou, C.; van Duin, A. Investigation of Complex Iron Surface Catalytic Chemistry Using the ReaxFF Reactive Force Field Method. *JOM* **2012**, *64*, 1426−1437.

(16) Schneider, J.; Hamaekers, J.; Chill, S. T.; Smidstrup, S.; Bulin, J.; Thesen, R.; Blom, A.; Stokbro, K. ATK-ForceField: A New Generation Molecular Dynamics Software Package. *Model. Simul. Mater. Sci. Eng.* **2017**, *25*, No. 085007.

(17) Smidstrup, S.; Pedersen, A.; Stokbro, K.; Jónsson, H. Improved Initial Guess for Minimum Energy Path Calculations. *J. Chem. Phys.* **2014**, *140*, No. 214106.

(18) Wert, C. A. Diffusion Coefficient of C in α-Iron. *Phys. Rev.* **1950**, *79*, No. 601.

(19) Soisson, F.; Becquart, C. S.; Castin, N.; Domain, C.; Malerba, L.; Vincent, E. Atomistic Kinetic Monte Carlo Studies of Microchemical Evolutions Driven by Diffusion Processes under Irradiation. *J. Nucl. Mater.* **2010**, *406*, 55−67.

(20) Rüger, R.; Yakovlev, A.; Philipsen, P.; Borini, S.; Melix, P.; Oliveira, A. F.; Franchini, M.; van Vuren, T.; Soini, T.; de Reus, M.; Ghorbani Asl, M.; Teodoro, T. Q.; McCormack, D.; Patchkovskii, S. *AMS DFTB 2019.3, SCM, Theoretical Chemistry*; Vrije Universiteit: Amsterdam, The Netherlands, 2019.

(21) Wang, J.; Wolf, R. M.; Caldwell, J. W.; Kollman, P. A.; Case, D. A. Development and Testing of a General Amber Force Field. *J. Comput. Chem.* **2004**, *25*, 1157−1174.

(22) Vanommeslaeghe, K.; Hatcher, E.; Acharya, C.; Kundu, S.; Zhong, S.; Shim, J.; Darian, E.; Guvench, O.; Lopes, P.; Vorobyov, I. CHARMM General Force Field: A Force Field for Drug-like Molecules Compatible with the CHARMM All-atom Additive Biological Force Fields. *J. Comput. Chem.* **2010**, *31*, 671−690.

(23) van Duin, A. *ReaxFF User Manual*; California Institute of Technology—Materials and Process Simulation Center, 2002.

(24) Deringer, V. L.; Csányi, G. Machine Learning Based Interatomic Potential for Amorphous Carbon. *Phys. Rev. B* **2017**, *95*, No. 094203.

(25) Dragoni, D.; Daff, T. D.; Csányi, G.; Marzari, N. Achieving DFT Accuracy with a Machine-Learning Interatomic Potential: Thermomechanics and Defects in BCC Ferromagnetic Iron. *Phys. Rev. Mater.* **2018**, *2*, No. 013808.

(26) Zhang, Y.; Lunghi, A.; Sanvito, S. Pushing the Limits of Atomistic Simulations towards Ultra-High Temperature: A Machine-Learning Force Field for ZrB2. *Acta Mater.* **2020**, *186*, 467−474.

(27) Aktulga, H. M.; Fogarty, J. C.; Pandit, S. A.; Grama, A. Y. Parallel Reactive Molecular Dynamics: Numerical Methods and Algorithmic Techniques. *Parallel Comput.* **2012**, *38*, 245−259.

(28) Kamat, A. M.; van Duin, A. C. T.; Yakovlev, A. Molecular Dynamics Simulations of Laser-Induced Incandescence of Soot Using an Extended ReaxFF Reactive Force Field. *J. Phys. Chem. A* **2010**, *114*, 12561−12572.

(29) Williams, L. R.; Dykhno, L. A.; Hanratty, T. J. Droplet Flux Distributions and Entrainment in Horizontal Gas-Liquid Flows. *Int. J. Multiphase Flow* **1996**, *22*, 1−18.

(30) Chun, C. M.; Mumford, J. D.; Ramanarayanan, T. A. Mechanisms of Metal Dusting Corrosion of Iron. *J. Electrochem. Soc.* **2002**, *149*, B348−B355.

(31) Chakrabarty, A.; Bentria, E. T.; Omotayo, S. A.; Bouhali, O.; Mousseau, N.; Becquart, C. S.; El Mellouhi, F. Elucidating the Role of Extended Surface Defects at Fe Surfaces on CO Adsorption and Dissociation. *Appl. Surf. Sci.* **2019**, *491*, 792−798.

(32) Chakrabarty, A.; Bouhali, O.; Mousseau, N.; Becquart, C. S.; Mellouhi, F. El. Insights on Finite Size Effects in Ab-Initio Study of

CO Adsorption and Dissociation on Fe 110 Surface. *J. Appl. Phys.* **2016**, *120*, No. 055301.
(33) Stukowski, A. Visualization and Analysis of Atomistic Simulation Data with OVITO−the Open Visualization Tool. *Model. Simul. Mater. Sci. Eng.* **2010**, *18*, No. 015012.
(34) Li, D. Molecular Dynamics Simulations: Analysis for Characterizing Simulated Atomic-Scale Defects in Crystal, and Kinetic Analysis of Ethylene-Propylene Diene-Terpolymer (EPDM) Pyrolysis Using ReaxFF; 2017.
(35) Chakrabarty, A.; Bouhali, O.; Mousseau, N.; Becquart, C. S.; El-Mellouhi, F. Influence of Surface Vacancy Defects on the Carburisation of Fe 110 Surface by Carbon Monoxide. *J. Chem. Phys.* **2016**, *145*, No. 044710.
(36) Nava Paz, J. C.; Grabke, H. J. Metal dusting. *Oxid. Met.* **1993**, *39*, 437.
(37) Pippel, E.; Woltersdorf, J.; Schneider, R. Micromechanisms of Metal Dusting on Fe-base and Ni-base Alloys. *Mater. Corros.* **1998**, *49*, 309−316.
(38) Bhadeshia, H. Cementite. *Int. Mater. Rev.* **2020**, *65*, 1−27.
(39) Grabke, H. J.; Müller-Lorenz, E. M.; Schneider, A. Carburization and Metal Dusting on Iron. *ISIJ Int.* **2001**, *41*, S1−S8.
(40) Rajeshwaran, K.; Karthikeyan, B. Density Functional Theoretical Studies of Some Novel Divalent Cation-Peptide Hybrid Models. *J. Comput. Theor. Nanosci.* **2019**, *16*, 1632−1639.
(41) Data retrieved from the Materials Project 2020.09.08 for Fe3C (mp-510623, DOI: 10.17188/1263035).

https://dx.doi.org/10.1021/acs.jpcc.0c09001
J. Phys. Chem. C 2020, 124, 28569−28579